BB

GSI

GSI-Preprint-96-21
MAI 1996

CHARGE-CHANGING NUCLEAR REACTIONS OF RELATIVISTIC LIGHT-ION BEAMS ($5 \leq Z \leq 10$) PASSING THROUGH THICK ABSORBERS*

I. Schall, D. Schardt, H. Geissel, H. Irnich, E. Kankeleit, G. Kraft, A. Magel, M.F. Mohar, G. Münzenberg, F. Nickel, C. Scheidenberger, W. Schwab

(Accepted for publication in Nucl. Instrum. Meth. B)

Gesellschaft für Schwerionenforschung mbH
Postfach 110552 · D-64220 Darmstadt · Germany

Charge-changing nuclear reactions of relativistic light-ion beams ($5 \leq Z \leq 10$) passing through thick absorbers [+]

I. Schall, D. Schardt, H. Geissel, H. Irnich, E. Kankeleit, G. Kraft, A. Magel, M.F. Mohar, G. Münzenberg, F. Nickel, C. Scheidenberger, W. Schwab Biophysik, Gesellschaft für Schwerionenforschung, 64291 Darmstadt, Germany*

** Institut für Kernphysik, Technische Hochschule, 64289 Darmstadt, Germany*

Abstract

Light-ion beams of ^{20}Ne, ^{19}Ne, ^{18}F, ^{16}O, ^{15}O, ^{14}N, ^{12}C, and ^{10}B in the energy range between 200 and 670 MeV/u were fragmented in thick targets of water, carbon, lucite, polyethylene, and aluminum. The nuclear charge composition of the fragmented beam was measured via energy loss in a large-area ionisation chamber. Using a water absorber of variable thickness up to 25 cm the elemental fragment yields were measured down to Z=5. Their build-up and decay characteristics are described by a system of differential equations. From the analysis of the depth-distributions of the surviving projectiles and the lower-Z projectile fragments, both total and partial charge-changing cross sections were obtained.

1 Introduction

Light-ion beams like ^{12}C, ^{14}N, ^{16}O, ^{20}Ne with kinetic energies of a few hundred MeV/u offer favourable conditions for the treatment of deep-seated tumors in cancer therapy [1, 2, 3]. Clinical trials were performed since 1977 at LBL Berkeley where about 500 patients have been treated [4, 5, 6] with neon and other ions heavier than helium until the closure of the BEVALAC in 1993. Therapy with carbon ions has started in 1994 at the dedicated medical facility HIMAC [7, 8, 9] at Chiba/Japan. Light ions exhibit an excellent physical depth-dose profile (Bragg curve) and in addition combine a low relative biological effectiveness (RBE) in the plateau of the Bragg curve and an increased RBE in the Bragg peak region. Therefore, the healthy tissue is only stressed by a relatively low

[+] part of the Ph.D thesis of I. Schall

dose inducing mostly repairable damage, whereas the tumor is exposed to a much greater dose that induces a large fraction of irrepairable damage. To some extent these excellent properties are deteriorated by nuclear fragmentation that occurs along the beam path and may cause a significant alteration of the radiation field due to the loss of primary beam particles and the build-up of lower-Z fragments. The lower-Z beam fragments in general have longer ranges and cause an unwanted dose contribution beyond the Bragg maximum of the primary ions. In the target volume the biological effect is reduced because only a fraction of the primary particles with a high stopping power (high-LET particles) reaches the Bragg maximum without fragmentation. The importance of these effects generally increases as a function of penetration depth. For a ^{20}Ne beam of 400 MeV/u, for example, only 40 percent of the primary particles reach the Bragg maximum at about 16 cm depth in water [10]. The physical beam models used e.g. in treatment planning programs therefore have to take into account these effects and require knowledge of the fragmentation process.

Since the discovery of heavy nuclei in the cosmic radiation [11] fragmentation reactions have been extensively studied for many years [12, 13]. Experimental data are available for many projectile-target combinations and for a wide range of beam energies. Dedicated studies of the fragmentation of light ions in water or other tissue-substitute material and its biomedical implications began at Princeton [14] and were performed for many years at LBL Berkeley in the course of the heavy-ion cancer treatment program. Maccabee et al. [15] measured the attenuation of an $^{16}_{8}$O beam of 233 MeV/u and the build-up of particles with Z=7, 6, 5 in water using silicon detectors for the Z-identification. From these data total and also partial charge-changing cross sections were deduced, the latter however with large uncertainties due to missing cross sections for secondary reactions. Schimmerling et al. [16] carried out detailed measurements on the characterization of 670 MeV/u ^{20}Ne beams, which were most frequently used for patient treatments at the BEVALAC. They obtained particle fluences and LET-distributions as a function of depth in water, using a complex beam spectrometer [17] with small detectors in the center of broad beams. Using calculated acceptance corrections [18] the fluence and LET data were compared [19, 20] with transport theories developed by Wilson et al. [21, 22]. Llacer et al. [23, 24, 25] performed measurements with a simpler solid-state telescope, which was

designed to obtain rapid information about the particle composition of fragmented beams. From the measured Z-distributions as a function of depth in water total charge-changing reaction cross sections were determined for ^{20}Ne and ^{28}Si beams of 670 MeV/u. Partial charge-changing cross sections were estimated for Z=9, 8, 7, 6 for a thin target approximation neglecting higher fragment generations.

Besides these studies which provided experimental data relevant for biomedical applications, much work has been devoted to the measurement of fragmentation cross sections (see e.g. refs. 26-31). We mention the detailed studies on charge- and mass-changing reaction cross sections for 1.88 GeV/u ^{56}Fe on ten different targets performed by Westfall et al. in 1979 [26]. More recently, comprehensive cross section data sets were reported by Webber et al. [29] (carbon to nickel beams on targets of hydrogen, helium, and carbon) and by Cummings et al. [30] for heavier beams. Fragmentation cross sections for charge-changing nuclear collisions were also obtained from measurements with nuclear track detectors [32, 33].

The database for biomedical applications, however, is still rather limited. In particular, fluence data for thick tissue equivalent targets are needed for dose and RBE calculations with ion beams. In this work, which is part of the physical program of the light-ion therapy project [34] at GSI, we present experimental data on the fragmentation of light-ion beams ($5 \leq Z \leq 10$) in water and various other materials. From the analysis of the elemental fragment distributions as a function of depth in water we obtained total and partial charge-changing reaction cross sections.

2 Experimental

Our measurements were carried out at the fragment separator (FRS) [35] which is part of the heavy-ion accelerator facility at GSI. The FRS is a magnetic forward spectrometer used to separate ion beams in flight based on magnetic analysis in combination with energy loss in matter [36]. We made use of the FRS in order to produce A/Z=2 nuclei as secondary beams from the fragmentation of a primary ^{18}O-beam in a 1 g/cm^2 beryllium target. In this way it was possible to study the fragmentation characteristics of beams of ^{16}O, ^{14}N, ^{12}C, and ^{10}B in various materials simultaneously and under identical exper-

imental conditions. Our experimental set-up was positioned at the final focus where a clean isotopic identification of each projectile was obtained from the measured energy loss in a large-area ionisation chamber [37] and time-of-flight through the separator (Fig. 1, left part). The particle trajectory was followed by measuring its position with multiwire chambers and in the horizontal plane also with the ionisation chamber (drift time). Fig. 1 (right part) shows the position in the direction of dispersion of the FRS of all produced A/Z=2 beams before hitting a water target of variable thickness or targets of aluminum and lucite in a distance of 1.5 m. In vertical direction the secondary beams had a width of typically 1 cm fwhm. Directly behind the target the Z-identification of the outgoing fragments was obtained by an energy-loss measurement in the ionisation chamber and a plastic-scintillator paddle (Fig. 2). The ionisation chamber was operated with a gas mixture of 90% argon and 10% methane at 1 atm. The active thickness was about 60 mg/cm^2 and the active area 20×20 cm^2. The scintillator (NE102A) was 9 mm thick and the area was a regular hexagon with maximal 12.5 cm in diameter which was coupled to a photo multiplier (EMI9954Q).

With this set-up we investigated the fragmentation characteristics of ^{18}F (671 MeV/u), ^{16}O (672 MeV/u), ^{14}N (674 MeV/u), ^{12}C (676 MeV/u), and ^{10}B (676 MeV/u) behind water targets with a thickness of 4.26, 8.51, 17.02, 25.54 g/cm^2, an aluminum target (5.54 g/cm^2) and a lucite target ($O_2C_5H_8$, 3.61 g/cm^2). Lower energy A/Z=2 beams ^{16}O (300 MeV/u), ^{14}N (303 MeV/u) and ^{12}C (305 MeV/u) were measured behind thick water targets of 4.26 and 8.51 g/cm^2. We also investigated the fragmentation of radioactive beams of ^{19}Ne (400 MeV/u), and ^{15}O (463 MeV/u) in direct comparison with their neighbouring stable isotopes ^{20}Ne (405 MeV/u) and ^{16}O (469 MeV/u), respectively. The neon and oxygen isotopes were measured behind 7.28, 10.08, 12.08 g/cm^2 and 4.26, 8.51, 12.77 g/cm^2 water, respectively.

Additional measurements of total charge-changing reaction cross sections were performed at the biophysics cave, using ^{12}C beams with kinetic energies of 192, 267, and 498 MeV/u delivered directly from the synchrotron SIS. The beam particles passed through a thin vacuum window (steel 200 μm thickness) and were counted in a NE102A plastic scintillator (1.5 mm thick) in front of a thick target. The surviving Z=6 particles behind the target were identified by their energy loss in a NE102A plastic scintillator of 9 mm thick-

ness. The targets consisted of 4.12 g/cm^2 lucite, 5.54 g/cm^2 aluminum, 4.26 g/cm^2 water, 3.82 g/cm^2 polyethylene (CH_2), and 7.28 g/cm^2 carbon. In all our measurements the data were processed by CAMAC-based ADC'S, QDC's and scalers and recorded event-by-event using the GSI on-line data acquisition sytem GOOSY [38].

3 Results

3.1 Nuclear charge distribution of fragmented light-ion beams

Projectile-like fragments are produced in peripheral collisions where only a few nucleons are abraded from the projectile nucleus. These fragments are emitted in a narrow forward cone and have about the same velocity as the projectile and a very small momentum spread due to the reaction process itself [39]. The energy loss ΔE_f of fragments passing with the velocity v through an ionization chamber scales with Z_f^2 and a velocity dependence f(v). The velocity spread of fragments produced in thick targets is mainly due to the fact that the nuclear reaction can take place at any depth in the absorber. For absorber thicknesses corresponding to the 'plateau' region of the Bragg curve – as used in the present work – the variation of the velocity dependence f(v) is still sufficiently small to permit an unambigious identification of Z_f by the measured ΔE_f alone (in the vicinity of the Bragg peak, however, an additional measurement of the velocity v_f becomes indispensable). An example of a nuclear charge distribution measured with the ionisation chamber for a primary ^{20}Ne beam is shown in Fig.3. The large peak at the upper end of the spectra corresponds to the nuclear charge of the primary beam projectiles which have passed through the absorber. However, this peak also includes a small contribution from neutron-deficient isotopes (e.g. ^{19}Ne, ^{18}Ne from ^{20}Ne projectiles) where only neutrons were lost due to nuclear reaction. Such type of reactions which have a probability of a few percent are termed 'non charge-changing reactions', in contrast to the 'charge-changing reactions' where fragments with a lower nuclear charge are produced. In the energy loss spectrum obtained with the ionisation chamber (Fig.3) projectile fragments with a nuclear charge down to Z=5 are observed with a typical resolution of ΔZ=0.3 to 0.5 (FWHM). In general, the heavier projectile fragments are accompanied by one or several light particles (in particular protons and α particles), which pass through the

ionisation chamber at the same time. Their contribution to the total energy-loss signal is very small due to the Z_f^2-scaling ('leading charge effect' [26]). There is no evidence for the production of accompanying heavier fragments (see e.g. [40]). Therefore, the peaks representing smaller energy depositions than that of the primary beam can be safely assigned to projectile-like fragments with correspondingly lower Z_f. Because of the large active area of the ionisation chamber and the sharply forward peaked angular distributions, acceptance corrections were not needed for the determination of elemental yields for $Z_f \geq 5$. The analysis of the corresponding scintillator data, which include the lighter fragments down to Z=1 but require calculated acceptance corrections, is still in progress.

3.2 Total charge-changing cross sections

In a first series of measurements using the setup shown in Fig.2 total charge-changing cross sections $\sigma_{\Delta Z}^{tot.}$ were obtained for various light-ion beams (^{10}B to ^{20}Ne) passing through thick water absorbers. The number of incident beam particles N_0 was obtained from the 'beam selection detector'. Behind the water absorber the number of 'surviving' beam particles N_s (for which the initial nuclear charge is conserved) was determined from the ΔE spectrum of the second ionisation chamber and normalized to N_0 to get the relative number $N_Z = N_s/N_0$ as a function of absorber depth x. Assuming that the nuclear reaction cross section is energy independent, this number is approximately given by

$$N_Z(x) = N_Z(0)e^{-\frac{x}{\lambda_Z}} \tag{1}$$

where λ_Z is the mean free path for a charge-changing reaction. For one specific absorber material an effective total charge-changing cross section is defined by

$$\sigma_{\Delta Z}^{tot.} = \frac{1}{N_M \lambda_Z} \tag{2}$$

where N_M is the number of atoms or molecules per unit volume of the absorber material.

$$N_M = \frac{N_A \rho}{M} \tag{3}$$

N_A is the Avogadro number, ρ the absorber mass density and M the atomic or molecular mass in atomic units. We note that the relative number of primary beam particles at zero water depth $N_Z(0)$ is slightly smaller than 100% due to some additional material (TOF

stop detector, air gaps) between the first ionisation chamber and the water absorber. The mean free path, λ_Z, was determined from the slope of the exponential function (1) which was fitted to the experimental data. Examples of the data are shown in Figs. 4 and 5, the results are compiled in Table 1. For ^{20}Ne the mean free path λ=166(4) mm is in agreement with our earlier measurement [10] which gave a value of 163(8) mm (E_{in}-E_{out}: 396-204 MeV/u). Previous measurements of λ for ^{20}Ne in water were carried out with 670 MeV/u beams at the BEVALAC. Llacer et al. reported values of 198 mm [23] and 154 mm [24]. The two results were obtained with similar experimental set-ups and the inconsistency was not understood. The measurements of Schimmerling et al. [16] resulted in a value of 160.7 mm. A later analysis of these experiments yielded a value of 165(12) mm [20]. Of these previous results only the first one of Llacer et al. disagrees with our measurements. Our results for ^{16}O beams can be compared to an early measurement at Berkeley's Bevatron by Maccabee et al. [15]. The value of 193(12) mm for a 233 MeV/u ^{16}O beam (E_{out}: 125 MeV/u) is somewhat lower than our value of 215(4) obtained at 300 MeV/u (E_{out}: 168 MeV/u). This may be explained by an increase of the reaction cross sections at low kinetic energies. Comparing beams of neighbouring isotopes (^{16}O, ^{15}O and ^{20}Ne, ^{19}Ne) with the same proton number no significant difference of the $\sigma^{tot}_{\Delta Z}$-values is found (see Fig.5 and Table 1).

In Fig.6 we compare those $\sigma^{tot}_{\Delta Z}$-values of Table 1 which were obtained at several beam energies with predictions of the semiempirical formulas of Sihver et al. [41]. We have chosen this model because it was developed especially for light projectile-target combinations ($Z \leq 26$) and its parameters were fitted to cross section data in this region. The total reaction cross section formula for nucleus-nucleus reactions used in [41] is based on the Bradt-Peters law [42] and assumes energy independence for incidident energies above 100 MeV/u. Similar expressions of the Bradt-Peters type were developed in many other works (see e.g. [19,40,43-46]). The procedure for calculating projectile fragment production cross sections by scaling semiempirical proton-nucleus partial cross sections is based on the work of Silberberg and Tsao [47]. The scaling algorithm [48] includes the weak factorization property [27] of projectile fragments. As can be seen from Fig.6 the predicitions of Sihver et al. [41] for the total charge-changing cross sections are in good agreement with our data. The slight increase of the cross sections towards higher energies

is well reproduced.

In another series of measurements in the biophysics cave we obtained mean free path lengths for ^{12}C beams passing through single thick absorbers of water, lucite, carbon, polyethylene, and aluminum. The numbers of incident beam particles and 'surviving' carbon particles leaving the absorber were obtained from the energy loss signals of two scintillation detectors. The mean free path lengths were evaluated from equation (1)

$$\lambda_Z = \frac{x}{ln\frac{N_Z(0)}{N_Z(x)}} \tag{4}$$

The fragmentation in the vacuum window and the first scintillator was taken into account by normalization measurements without absorber for each beam energy where numbers in the order of 0.96 were found for $N_Z(0)$. Table 2 compiles the results for carbon beams at different kinetic energies of the incident beam particles. Similar to the results shown in Fig. 6 there is a slight increase for $\sigma_{\Delta Z}^{tot}$ towards high energies and also below about 200 MeV/u. Furthermore we obtained results for ^{16}O, ^{14}N, and ^{12}C beams passing through aluminum and lucite absorbers (Table 3). For lucite absorbers the cross sections can also be obtained from the following combination:

$$\sigma(lucite) = 2\sigma(H_2O) + 2\sigma(CH_2) + 3\sigma(C) \tag{5}$$

by adding the cross sections as shown in Table 4. The total charge-changing cross sections for water, polyethylene, and carbon were taken from this work and from earlier measurements of Webber et al. [29] (E_{in}: 610 MeV/u ^{12}C on 11.08 g/cm^2 polyethylene and 12.73 g/cm^2 carbon, 550 MeV/u ^{14}N on 6.01 g/cm^2 polyethylene and 7.03 g/cm^2 carbon, 640 MeV/u ^{12}C on 8.75 g/cm^2 polyethylene and 10.01 g/cm^2 carbon). Except for ^{16}O beam, where the 'combined' cross section is 5% lower than the direct measurement, the cross sections obtained by combination agree within the uncertainties with the direct measurement. We note that from the cross sections for H_2O, CH_2, and C targets the cross sections for H and O targets can be obtained from

$$\sigma(CH_2) - \sigma(C) = \sigma(H_2); \qquad \sigma(H_2O) - \sigma(H_2) = \sigma(O) \tag{6}$$

Then, in principle, the cross section for any combined target containing these elements can be evaluated.

3.3 Partial charge-changing cross sections

Partial charge-changing cross sections $\sigma_{\Delta Z}^{part.}$ for the production of lower-Z fragments (Z>4) from beams of 670 MeV/u ^{16}O, ^{14}N, and ^{12}C were obtained from the analysis of the measured build-up characteristics in a water absorber. At each water depth the fragment yield for a given Z_f was normalized to the number of incoming beam particles. The resulting depth distributions are shown in Fig. 7. Mathematically these build-up and decay curves can be described by solutions of a diffusion equation, the so-called 'transport equation'. This is well known from cosmic ray calculations where diffusion equations were applied to the transport of galactic cosmic rays through the atmosphere [49]. Allkofer and Heinrich [50] obtained relative fragmentation probabilities in air using an analytical solution of a one-dimensional transport equation. Wilson et al. [51, 52] presented a comprehensive physical model for galactic heavy ion propagation based on the Boltzmann transport equation. In the following we make the simplifying assumption that the charge-changing fragmentation cross sections are independent of the energy, which seems to be justified for energies $E > 100$ MeV/u. Furthermore we assume that these cross sections can also be applied to secondary and higher-generation fragments (neglecting a possible dependence on their isotopic distributon). Then the elemental fragment distributions as a function of absorber depth x can be described by a homogeneous system of differential equations which looks in matrix form:

$$\begin{pmatrix} \frac{d}{dx}N_Z(x) \\ \frac{d}{dx}N_{Z-1}(x) \\ \vdots \\ \frac{d}{dx}N_{Z-n}(x) \end{pmatrix} = \begin{pmatrix} -\lambda_Z^{-1} & 0 & \cdots & 0 \\ \lambda_{Z,Z-1}^{-1} & -\lambda_{Z-1}^{-1} & \ddots & \vdots \\ \cdots & & \ddots & 0 \\ \lambda_{Z,Z-n}^{-1} & \lambda_{Z-1,Z-n}^{-1} & \cdots & -\lambda_{Z-n}^{-1} \end{pmatrix} \times \begin{pmatrix} N_Z(x) \\ N_{Z-1}(x) \\ \vdots \\ N_{Z-n}(x) \end{pmatrix} \tag{7}$$

or in an abbreviated form:

$$\frac{d}{dx}N(x) = LN(x). \tag{8}$$

where $N_Z(x)$ is the relative number of beam particles conserving the nuclear charge and $N_{Z-i}(x)$ is the relative number of fragments which have i protons less than the primary ion. The diagonal elements λ_Z^{-1} and λ_{Z-i}^{-1} in the matrix correspond to the <u>total</u> charge-changing cross sections (see equation 2) of the incident beam particles and of lower Z-fragments. The lower diagonal elements $\lambda_{Z-i,Z-j}^{-1}$ are proportional to the <u>partial</u> charge-changing cross

sections. In previous works, Maccabee et al. [15] and Llacer et al. [24] fitted the fragment yields as a function of the absorber depth with a solution of differential equations in order to obtain partial charge-changing cross sections. However, they took into account only the first fragment generation using as a fit function a solution of equation

$$\frac{d}{dx}N_{Z-i}(x) = \lambda_{Z,Z-i}^{-1}N_Z(x) - \lambda_{Z-i}^{-1}N_{Z-i}(x). \tag{9}$$

Because there were no experimental data for the mean free paths λ_{Z-i} of the fragments, Maccabee et al. estimated the missing values from a geometrical scaling ($\propto A^{2/3}$) of the measured mean free path length of the primary 233 MeV/u ^{16}O beam and fitted the fragment yields at relatively small depths in water. As was shown by Llacer et al. [24] for a 670 MeV/u $^{20}_{10}Ne$ beam, the fit to the lower-Z fragment yields ($Z_f \leq 8$) failed at larger depths due to the influence of higher fragment generations. They obtained partial charge-changing cross sections only from a thin-target approximation neglecting $\lambda_{Z-i}^{-1}N_{Z-i}(x)$. Because of the lower triangular form of matrix L, the eigenvalues of L are the diagonal elements themselves. Thus a solution of equation (7) is:

$$\begin{pmatrix} N_1(x) \\ N_2(x) \\ \vdots \\ N_n(x) \end{pmatrix} = \begin{pmatrix} a_{11} & 0 & \cdots & 0 \\ a_{21} & a_{22} & 0 & \vdots \\ \vdots & & \ddots & 0 \\ a_{n1} & a_{n2} & \ldots & a_{nn} \end{pmatrix} \times \begin{pmatrix} exp(-l_{11}x) \\ exp(-l_{22}x) \\ \vdots \\ exp(-l_{nn}x) \end{pmatrix} \tag{10}$$

or in an abbreviated form:

$$N(x) = A\ exp(-lx) \tag{11}$$

where the fragment yields $N_{Z-i}(x)$ are represented as linear combinations of exponential functions. The parameters a_{ij} can be obtained from a fit to the elemental fragment yields which were measured at five different water depths. Our analysis procedure differs at this point from the one described in [26], where the elemental fragment yields were measured for a single target thickness and an exponential power series of matrix L was used for the solution of equation (9). Assuming that matrix A and all parameters l_{ii} were determined by fitting all $N_{Z-i}(x)$ curves of one fragmented beam, matrix L containing the partial cross sections can be determined in the following way. Differentiation of equation (10)

results in:

$$\begin{pmatrix} \frac{d}{dx}N_1(x) \\ \frac{d}{dx}N_2(x) \\ \vdots \\ \frac{d}{dx}N_n(x) \end{pmatrix} = \begin{pmatrix} a_{11} & 0 & \cdots & 0 \\ a_{21} & a_{22} & \ddots & \vdots \\ \vdots & & \ddots & 0 \\ a_{n1} & a_{n2} & \cdots & a_{nn} \end{pmatrix} \times \begin{pmatrix} -l_{11} & 0 & \cdots & 0 \\ 0 & -l_{22} & \ddots & \vdots \\ \vdots & 0 & \ddots & 0 \\ 0 & \cdots & 0 & -l_{nn} \end{pmatrix} \times \begin{pmatrix} exp(-l_{11}x) \\ exp(-l_{22}x) \\ \vdots \\ exp(-l_{nn}x) \end{pmatrix} \tag{12}$$

or abbreviated:

$$\frac{d}{dx}N(x) = A\ L_D\ exp(-lx). \tag{13}$$

With equations (11) and (13) the differential equation (8) becomes:

$$A\ L_D\ exp(-lx) = L\ A\ exp(-lx) \tag{14}$$

$$A\ L_D = L\ A \tag{15}$$

$$A\ L_D\ A^{-1} = L. \tag{16}$$

According to equation (16) matrix L can in principle be calculated in an elegant way by a simple matrix operation. In turn, when all cross sections in matrix L are known, the fragment depth distributions can be calculated for any beam composition in front of the absorber in the following way. Using equation (15) and the definition

$$\tilde{L} \equiv L - L_D \tag{17}$$

$$\tilde{L}\ A = A\ L_D - L_D\ A \tag{18}$$

or explicitely for each matrix element

$$\sum_{k=0}^{i-(j+1)} l_{i,j+k}a_{j+k,j} = a_{ij}(l_{ii} - l_{jj}) \tag{19}$$

the lower diagonal elements of matrix A result out of

$$a_{ij} = \frac{1}{l_{ii} - l_{jj}} \sum_{k=0}^{i-(j+1)} l_{i,j+k}a_{j+k,j}. \tag{20}$$

The diagonal elements a_{ii} can be determined from equation (10):

$$a_{ii} = N_i(0) - \sum_{l=1}^{i-1} a_{il}. \tag{21}$$

In the following we apply the above outlined formalism to the specific fragmentation data shown in Figs.4 and 7. Using equation (10) the depth distributions $N_{Z-i}(x)$ for the fragmentation of primary ^{16}O, ^{14}N, ^{12}C, and ^{10}B ions are represented by linear combinations of exponential functions:

$$\begin{pmatrix} N_{Z=8}(x) \\ N_{Z=8-1}(x) \\ N_{Z=8-2}(x) \\ N_{Z=8-3}(x) \end{pmatrix} = \begin{pmatrix} a_{11} & 0 & 0 & 0 \\ a_{21} & a_{22} & 0 & 0 \\ a_{31} & a_{32} & a_{33} & 0 \\ a_{41} & a_{42} & a_{43} & a_{44} \end{pmatrix} \times \begin{pmatrix} exp(-\lambda_8^{-1}x) \\ exp(-\lambda_7^{-1}x) \\ exp(-\lambda_6^{-1}x) \\ exp(-\lambda_5^{-1}x) \end{pmatrix} \tag{22}$$

$$\begin{pmatrix} N_{Z=7}(x) \\ N_{Z=7-1}(x) \\ N_{Z=7-2}(x) \end{pmatrix} = \begin{pmatrix} b_{11} & 0 & 0 \\ b_{21} & b_{22} & 0 \\ b_{31} & b_{32} & b_{33} \end{pmatrix} \times \begin{pmatrix} exp(-\lambda_7^{-1}x) \\ exp(-\lambda_6^{-1}x) \\ exp(-\lambda_5^{-1}x) \end{pmatrix} \tag{23}$$

$$\begin{pmatrix} N_{Z=6}(x) \\ N_{Z=6-1}(x) \end{pmatrix} = \begin{pmatrix} c_{11} & 0 \\ c_{21} & c_{22} \end{pmatrix} \times \begin{pmatrix} exp(-\lambda_6^{-1}x) \\ exp(-\lambda_5^{-1}x) \end{pmatrix} \tag{24}$$

$$N_{Z=5}(x) = d_{11}exp(-\lambda_5^{-1}x) \tag{25}$$

The total number of 24 parameters $(a_{ij}, b_{ij}, c_{ij}, d_{ij}, \lambda_i)$ in equations (22) - (25) reduces to 20 through the relations

$$\begin{aligned} b_{21} &= b_{11}a_{32}/a_{22} \\ b_{31} &= b_{11}a_{42}/a_{22} \\ b_{32} &= b_{22}a_{43}/a_{33} \\ c_{21} &= c_{11}a_{43}/a_{33} \end{aligned} \tag{26}$$

These relations result from the simplifying assumption that the partial cross section for a given channel $Z_i \rightarrow Z_f$ is the same for primary particles as for secondary or higher generation particles with initial charge Z_i (neglecting a possible dependence on the mass number or mass distribution of secondary particles). For example, the matrix element l_{32} in case of ^{16}O-fragmentation is assumed to be identical with l_{21} in case of ^{14}N-fragmentation (see equation (7)):

$$\lambda_{Z-1,Z-2}^{-1}(\mathrm{Z=8}) \quad \equiv \quad \lambda_{Z,Z-1}^{-1}(\mathrm{Z=7}) \tag{27}$$

Application of equation (16) then leads to the relations (26). The remaining 20 free parameters were fitted simultaneously to the 50 data points shown in Figs. 4 and 7,

giving a χ^2_{min}-value of 18.7 for the best fit. Finally, the partial charge changing cross sections were obtained by the matrix operation (16). Their variances were determined by error propagation [53] as the diagonal elements of

$$(\frac{\partial l}{\partial \alpha})^T \; V_{\hat{\alpha}} \; \frac{\partial l}{\partial \alpha}|_{\hat{\alpha}} \tag{28}$$

where $\hat{\alpha} = (a_{11}, a_{21}, a_{22}, a_{31}, a_{32}, a_{33}, a_{41}, a_{42}, a_{43}, a_{44}, b_{11}, b_{22}, b_{33}, c_{11}, c_{22}, d_{11}, \lambda_5, \lambda_6, \lambda_7, \lambda_8)$ is the solution vector, $\partial l/\partial \alpha$ is the Jacobian matrix of $\lambda_{8,7}$, $\lambda_{8,6}$, $\lambda_{8,5}$, $\lambda_{7,6}$, $\lambda_{7,5}$, $\lambda_{6,5}$ and $(\partial l/\partial \alpha)^T$ its transpose. $V_{\hat{\alpha}}$ is the covariance matrix

$$V_{\hat{\alpha}} = 2(\frac{\partial^2 \chi^2}{\partial \alpha^2})^{-1}_{\hat{\alpha}} \tag{29}$$

where $\partial^2\chi^2/\partial\alpha^2$ is a 20×20 matrix with mnth element $\partial^2\chi^2/(\partial\alpha_n^2 \partial\alpha_m^2)$.

In Table 5 all charge-changing cross sections obtained for ^{16}O, ^{14}N, and ^{12}C beams at 670 MeV/u are compiled. Also shown in Table 5 are the predictions of the semiempirical formulas [41] (see above) and of a recently developed statistical abrasion model [54]. The oxygen data show about equal probabilities for the single and double charge removal, whereas a much higher probability for the single charge removal is predicted by the abrasion model [54]. The excess production of ^{12}C fragments in the ^{16}O fragmentation (double charge removal) can be explained by alpha clustering effects [55]. As was recently shown by Wilson et al. [56], the addition of the single alpha knockout cross section to the NUCFRG2-code [57] brings good agreement with our oxygen data and with earlier $^{16}\text{O} \rightarrow {}^{12}\text{C}$ fragmentation data [27].

Partial charge-changing cross sections for ^{16}O and ^{14}N beams in lucite and aluminum absorbers are given in Table 6. Since the absorbers used in these measurements were relatively thin (0.1-0.2 mean free paths) only the first fragment generation was taken into account. Then one obtains from equations (10), (20), (21)

$$N_2(x) = N_2(0)e^{-l_{22}x} + N_1(0)\frac{l_{21}}{l_{22} - l_{11}}[e^{-l_{11}x} - e^{-l_{22}x}]. \tag{30}$$

and the partial charge-changing cross sections are calculated as

$$\lambda^{-1}_{p,f} = \frac{\lambda_p^{-1} - \lambda_f^{-1}}{N_p(0)[e^{-\frac{x}{\lambda_p}} - e^{-\frac{x}{\lambda_f}}]}[N_f(x) - N_f(0)e^{-\frac{x}{\lambda_f}}]. \tag{31}$$

using the total charge-changing cross sections of Table 3. In case of oxygen on lucite the relative cross sections for single and double charge removal are similar to the values for water (cf. Table 5). The data for the aluminum target show an even smaller probability for single charge than for double charge removal.

The influence of higher fragment generations on the build-up and decay characteristics is illustrated in Fig. 8 using our experimental data for an ^{16}O beam of 672 MeV/u penetrating through 25 cm of water. The solid line is our fit result taking into account all fragment generations. To show the fragment production originating from the first generation only all matrix elements in equation (7) except the first column and the diagonal elements are put to zero. The corresponding yield curves for Z_f=5 and Z_f=6 are indicated as dashed lines. The deviation from the measured curves shows that for larger penetration depths (>5 cm in this example) the higher generations contribute significantly to the fragment build-up.

4 Conclusion

For medical applications of light-ion beams in radiation therapy good knowledge of the physical quantities involved in the interaction of these beams with tissue is a basic requirement. In the present work the attenuation of primary particles and the build-up of projectile fragments were investigated for ion beams in the range of ^{10}B to ^{20}Ne using water as a tissue equivalent material. The measured mean free path lengths and corresponding effective total charge-changing cross sections $\sigma_{\Delta Z}^{tot.}$ are of particular importance for the understanding of the detailed shape of depth-dose distributions (Bragg curves) [21,57-59]. Among our results the relatively high value of $\sigma_{\Delta Z}^{tot.}$ for ^{14}N is noticeable. On the other hand, the value for ^{12}C is very low (even lower than for ^{10}B), and therefore carbon ions from this point of view offer favourable conditions for the treatment of deep-seated tumors.

Under simplifying assumptions the build-up and decay characteristics of the lower-Z fragment intensities is mathematically described by a homogeneous system of differential equations. The elemental fragment yields as a function of water depths can be represented by linear combinations of exponential functions. It was shown that partial charge-changing

cross sections can be obtained by simple matrix operations from the corresponding fit parameters. Once the cross sections are known, an inverse procedure can be applied to calculate analytically the fragment intensities at any depth of the absorber including all fragment generations.

We would like to thank T. Brohm and L. Sihver for providing us with their model calculations and for many helpful discussions.

References

[1] C.A. Tobias and P.W. Todd, Heavy charged particles in cancer therapy, in *Radiobiology and Radiotherapy*, National Cancer Institute Monograph No.24, 1967.

[2] P.L.Petti and A.J. Lennox, Annu.Rev.Nucl.Part.Sci. 44 (1994) 155.

[3] U. Linz (Ed.), *Ion Beams in Tumor Therapy*, Chapmann & Hall, London, 1995.

[4] J.R. Castro, G.T.Y. Chen and E.A. Blakely, Radiat. Res. 104 (1985) S263.

[5] J.I. Fabricant, J.T. Lyman, K.A. Frankel, Radiat. Res. (Suppl. 104) 2 (1985) 244.

[6] D.E. Linstad, J.R. Castro, T.L. Philipps, Int. J. Radiat. Oncol. Biol. Phys. 20 (1991) 761.

[7] K. Kawachi, T. Kanai, M. Endo, Y. Hirao and H. Tsumenoto, J. Jpn. Soc. Ther. Radiol. Oncol. 1 (1989) 19.

[8] Y. Hirao, H. Ogawa, S. Yamada, Y. Sato, T. Yamada, K. Sato, A. Itano, M. Kanazawa, K. Noda, M. Kawachi, M. Endo, T. Kanai, T. Kohno, M. Sudou, S. Minohara, A. Kitagawa, F. Soga, E. Takada, S. Watanabe, K. Endo, M. Kumada, and S. Matsumoto, Nucl. Phys. A538 (1992) 541c.

[9] T. Kanai and E. Takada (Eds.), Proceedings of NIRS Int. Seminar on the Application of Heavy Ion Accelerator to Radiation Therapy of Cancer in connection with XXI PTCOG meeting, Nov. 14-16, 1994, NIRS, Chiba, Japan

[10] I. Schall, D. Schardt, H. Geissel, G. Kraft, A. Magel, M.F. Mohar, G. Münzenberg, F. Nickel, C. Scheidenberger, W. Schwab, E. Kankeleit, A. Fukumura, Radiat. Effects and Defects in Solids 126 (1993) 385.

[11] P. Frier, E.J. Lofgren, E.P. Ney, and F. Oppenheimer, Phys. Rev. 74 (1949) 1818; H.L. Bradt, ibid. 74 (1949) 213

[12] A.S. Goldhaber and H.H. Heckman, Ann. Rev. Nucl. Part. Sci. 28 (1978) 161.

[13] E.M. Friedlander and H.H. Heckman, in *Treatise on heavy-ion science*, Vol.4, ed. D.A. Bromley, Plemum, New York, 1985, p. 403.

[14] W. Schimmerling, K.G. Vosburgh, and P.W. Todd, Science 174 (1971) 1123.

[15] H.D. Maccabee and M.A. Ritter, Radiat. Res. 60 (1974) 409.

[16] W. Schimmerling, J. Miller, M. Wong, M. Rapkin, J. Howard, H.G. Spieler and B.V. Jarret, Radiat. Res. 120 (1989) 36.

[17] W. Schimmerling, T.S. Subramanian, W.J. McDonald, S.N. Kaplan, A. Sadoff and G. Gabor, Nucl. Instr. and Meth. 205 (1983) 531.

[18] W. Schimmerling, M. Rapkin, M. Wong, and J. Howard, Med. Phys. 13 (1986) 217.

[19] M.R. Shavers, S.B. Curtis, J. Miller, and W. Schimmerling, Radiat. Res. 124 (1990) 117.

[20] M.R. Shavers, K. Frankel, J. Miller, W. Schimmerling, L.W. Townsend, and J.W. Wilson, Radiat. Res. 136 (1993) 1.

[21] J.W. Wilson, H.B. Bidasaria, J. Howard, W. Schimmerling, L.W. Townsend, and M. Wong, Health Phys. 46 (1984) 1101.

[22] J.W. Wilson, L.W. Townsend, S.L. Lamkin, and B.D. Ganapol, Radiat. Res. 122 (1990) 223.

[23] J. Llacer, C.A. Tobias, W.R. Holley and T. Kanai, Med. Phys. 11 (1984) 266.

[24] J. Llacer, J.B. Schmidt and C.A. Tobias, Med. Phys. 17 (1990) 151.

[25] J. Llacer, J.B. Schmidt and C.A. Tobias, Med. Phys. 17 (1990) 158.

[26] G.D. Westfall, L.W. Wilson, P.J. Lindstrom, H.J. Crawford, D.E. Greiner, and H.H Heckman, Phys. Rev. C19 (1979) 1309.

[27] D.L. Olson, B.L. Berman, D.E. Greiner, H.H. Heckman, P.J. Lindstrom, and H.J. Crawford, Phys. Rev. C28 (1983) 1602.

[28] J.M. Kidd, P.J. Lindstrom, H.J. Crawford, and G. Woods, Phys. Rev. C37 (1988) 2613.

[29] W.R. Webber, J.C. Kish and D.A. Schrier, Phys. Rev. C41 (1990) 520; W.R. Webber, J.C. Kish and D.A. Schrier, ibid. C41 (1990) 533; W.R. Webber, J.C. Kish and D.A. Schrier, ibid. C41 (1990) 547;

[30] J.R. Cummings, W.R. Binns, T.L. Garrard, M.H. Israel, J. Klarmann, E.C. Stone, and C.J. Waddington, Phys. Rev. C42 (1990) 2508.

[31] C.J. Zeitlin, K.A. Frankel, W. Gong, L. Heilbronn, E.J. Lampo, R. Leres, J. Miller, and W. Schimmerling, Radiat. Meas. 23 (1994) 65.

[32] C. Brechtmann and W. Heinrich, Nucl. Instrum. Meth. B29 (1988) 675.

[33] J. Dreute et al., Phys. Rev. C44 (1991) 1057.

[34] *Einrichtung einer experimentellen Strahlentherapie bei der GSI Darmstadt*, Eds. G. Kraft and G. Gademann, GSI-Report 93-23 (May 1993).

[35] H. Geissel, P. Armbruster, K.-H. Behr, A. Brühnle, K. Burkhard, M. Chen, H. Folger, B. Franczak, H. Keller, O. Klepper, B. Langenbeck, F. Nickel, E. Pfeng, M. Pfuetzner, E. Roeckl, K. Rykaczewski, I. Schall, D. Schardt, C. Scheidenberger, K.-H. Schmidt, A. Schröter, T. Schwab, K. Sümmerer, M. Weber, G. Münzenberg, T. Brohm, H.G. Clerc, M. Fauerbach, J.-J. Gaimard, A. Grewe, E. Hanelt, B. Knödler, M. Steiner, B. Voss, J. Weckenmann, C. Ziegler, A. Magel, H. Wollnick, J.P. Dufour, Y. Fujita, D.J. Viera and B. Sherrill, Nucl. Instr. and Meth. B70 (1992) 286.

[36] J.P. Dufour, R. Del Moral, H. Emmermann, F. Hubert, D. Jaen, C.Poinot, M.S. Pravikoff, A. Fleury, H. Delagrange and K.-H. Schmidt, Nucl. Instr. and Meth. A248 (1986) 267.

[37] M. Pfützner, H. Geissel, G. Münzenberg, F. Nickel, Ch. Scheidenberger, K.-H. Schmidt, K. Sümmerer, T. Brohm, B. Voss and H. Bichsel, Nucl. Instr. and Meth. B86 (1994) 213

[38] H.G. Essel, H. Grein, T. Kroll, W. Kynast, M. Richter, H. Sohlbach, W. Spreng and K. Winkelmann, IEEE Trans. Nucl. Sci. NS-34 (4) (1987) 907.

[39] D.E. Greiner, P.J. Lindstrom, H.H. Heckman, B. Cork, and F.S. Beiser, Phys. Rev. Lett. 35 (1975) 152.

[40] H.H. Heckmann, D.E. Greiner, P.J. Lindstrom and H. Shwe, Phys. Rev. C17 (1976) 1735.

[41] L. Sihver, C.H. Tsao, R. Silberberg, T. Kanai and A.F. Barghouty, Phys. Rev. C47 (1993) 1225.

[42] H.L. Bradt and B. Peters, Phys. Rev. 77 (1950) 54.

[43] L.W. Townsend and J.W. Wilson, Radiat. Res. 106 (1986) 283.

[44] J.W. Wilson, L.W. Townsend, and F.F. Badavi, Nucl. Instrum. Meth. B18 (1987) 225.

[45] S. Kox, Phys. Rev. C35, (1987) 1678.

[46] K. Sümmerer, W. Brüchle, D.J. Morissey, M. Schädel, B. Szweryn, and Yang Weifan, Phys. Rev. C42 (1990) 2546.

[47] R. Silberberg and C.H. Tsao, Astrophys. J. Suppl. 25 (1973) 315; ibid. 25 (1973) 335.

[48] C.H. Tsao, R. Silberberg, A.F. Barghouty, L. Sihver, and T. Kanai, Phys. Rev. C47 (1993) 1257.

[49] M.M. Shapiro and R. Silberberg, Annu. Rev. Nucl. Sci. 20 (1970) 323.

[50] O.C. Allkofer and W. Heinrich, Nucl. Phys. B71 (1974) 429.

[51] J.W. Wilson, L.W. Townsend, and F. Badavi, Radiat. Res. 109 (1987) 173.

[52] J.W. Wilson, L.W. Townsend, W. Schimmerling, G.S. Khandelwal, F. Khan, J.E. Nealy, F.A. Cucinotta, L.C. Simonsen, J.L. Shinn, J.W. Norbury, *Transport methods and interactions for space radiation*, Washington DC, NASA Report No. 1257 (1991).

[53] Review of Particle Properties, Phys. Lett. 239 (1990) section III.28.

[54] T. Brohm and K.-H. Schmidt, Nucl. Phys A569 (1994) 821.

[55] F.A. Cucinotta, Bull. Am. Phys. Soc. 48 (1994) 1401.

[56] J.W. Wilson, F.A. Cucinotta, H. Tai, J.L. Shin, S.Y. Chun, R.K. Tripathi, L. Sihver, Fifth Workshop on Heavy Charged Particles in Biology and Medicine, GSI, Darmstadt, Aug. 23-25,1995; GSI-Report-95-10, p.193.

[57] J.W. Wilson, R.K. Tripathi, F.A. Cucinotta, J.L. Shinn, F.F. Badavi, S.Y. Chun, J.W. Norbury, C.J. Zeitlin, L. Heilbronn, and J. Miller, NASA TP-3533 (1995).

[58] W. Heinrich, Radiat. Effects 40 (1979) 167.

[59] J.W. Wilson, M. Reginatto, F. Hajnal, and S.Y. Chun, Health Phys. 68 (1995) 532.

[60] L. Sihver, D. Schardt, and T. Kanai, GSI Scientific Report 1993 (1994) 233.

Tables

Table 1: Mean free path lengths λ_Z and total charge-changing cross sections $\sigma_{\Delta Z}^{tot.}$ of several light-ion beams in water. E_{in} and E_{out} denote the kinetic energies of the primary beam particles at the entrance and the exit of the water absorber. ν is the degree of freedom, i.e. the number of data points minus two (the number of free parameters of the fit) and $P(\chi^2,\nu)$ the integral probability function of exceeding χ^2.

Beam	E_{in}-E_{out} [MeV/u]	ν	$P(\chi^2,\nu)$	λ_Z [mm]	$\sigma_{\Delta Z}^{tot.}$ [mb]
^{20}Ne	405-204	2	0.67	166(4)	1800(43)
^{19}Ne	400-183	2	0.22	163(4)	1834(45)
^{18}F	671-374	3	0.83	153(7)	1953(89)
^{16}O	300-168	1	0.65	215(4)	1390(26)
	469-310	2	0.06	202(2)	1480(15)
	672-413	3	0.16	193(1)	1549(8)
^{15}O	463-302	2	0.03	199(1)	1502(8)
^{14}N	303-199	1	0.07	209(6)	1430(41)
	674-451	3	0.83	199(2)	1502(15)
^{12}C	305-212	1	0.75	248(7)	1205(34)
	676-487	3	0.06	237(3)	1261(16)
^{10}B	676-520	3	0.96	223(6)	1340(36)

Table 2: Total charge-changing cross sections $\sigma_{\Delta Z}^{tot.}$ of ^{12}C beams in various target materials.

target	E_{in}=192 MeV/u		E_{in}=267 MeV/u		E_{in}=498 MeV/u	
material	E_{out}(MeV/u)	$\sigma_{\Delta Z}^{tot.}$/mb	E_{out}(MeV/u)	$\sigma_{\Delta Z}^{tot.}$/mb	E_{out}(MeV/u)	$\sigma_{\Delta Z}^{tot.}$/mb
lucite	128	7250(102)	218	6733(74)	464	7019(112)
water	124	1264(16)	215	1163(13)	462	1220(20)
carbon	76	893(12)	185	748(10)	443	758(15)
polyethylene	128	1157(19)	218	1075(11)	464	1135(15)
aluminum	126	1179(20)	216	1078(17)	462	1103(28)

Table 3: Total charge-changing cross sections $\sigma_{\Delta Z}^{tot.}$ of ^{16}O, ^{14}N, and ^{12}C beams in aluminum and lucite targets.

Beam	E_{in}(MeV/u)	aluminum		lucite	
		$\sigma_{\Delta Z}^{tot.}$/mb	E_{out}(MeV/u)	$\sigma_{\Delta Z}^{tot.}$/mb	E_{out}(MeV/u)
^{16}O	672	1297(51)	628	8607(240)	637
^{14}N	674	1223(130)	636	7910(240)	643
^{12}C	676	1096(100)	643	7170(360)	650

Table 4: Comparison of total charge-changing cross sections $\sigma_{\Delta Z}^{tot.}$ for a composite material (lucite) obtained from the combination of cross sections and from a direct measurement (last column); the values marked by an asterisk are from [29].

Beam	water		polyethylene		carbon			lucite
	2 $\sigma(H_2O)$	+ 2	$\sigma(CH_2)$	+ 3	σ(C)	=	$\sigma_{comb.}(O_2C_5H_8)$	$\sigma(O_2C_5H_8)$
^{16}O	1549(8)		1316(13)*		823(8)*		8199(66)	8607(240)
^{14}N	1502(15)		1251(13)*		796(8)*		7894(80)	7910(240)
^{12}C	1261(16)		1125(11)*		699(7)*		6869(75)	7170(360)
^{12}C	1220(20)		1135(15)		758(15)		6984(115)	7019(112)

Table 5: Total and partial charge-changing cross sections obtained for ^{16}O, ^{14}N, and ^{12}C beams at 670 MeV/u in water. The relative charge removal probabilities are compared to the model predictions of Sihver et al. [41] and Brohm et al. [54].

Beam	ΔZ	σ/mb	%	Sihver et al.	Brohm et al.
^{16}O	total	1549(8)	= 100.0		
	1	269(5)	17.4	[20.0]	[30.6]
	2	275(5)	17.8	[17.1]	[17.7]
	3	130(5)	8.4	[8.9]	[8.4]
^{14}N	total	1502(15)	= 100.0		
	1	339(9)	22.6	[18.3]	[28.7]
	2	138(7)	9.2	[9.8]	[13.1]
^{12}C	total	1261(16)	= 100.0		
	1	215(6)	17.0	[17.7]	[43.2]

Table 6: Total and partial charge-changing cross sections obtained for ^{16}O and ^{14}N beams ($E_{in} \sim 670$MeV/u) in aluminum and lucite.

Beam	ΔZ	aluminum		lucite	
		σ/mb	%	σ/mb	%
^{16}O	total	1297(51)	= 100.0	8607(240)	= 100.0
	1	162(11)	12.5	1450(50)	16.8
	2	231(16)	17.8	1450(50)	16.8
^{14}N	total	1223(130)	= 100.0	7910(240)	= 100.0
	1	190(39)	15.5	1660(170)	21.0

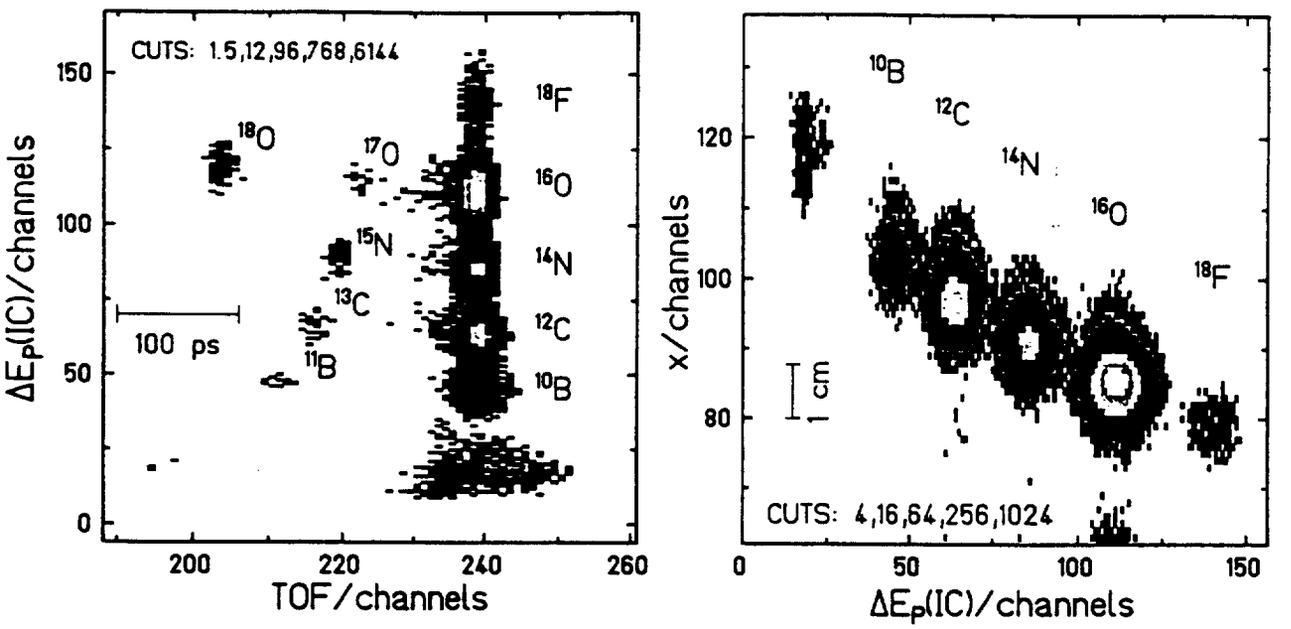

Fig. 1: Secondary beams produced by the fragmentation of an ^{18}O beam of 702 MeV/u in a 1 g/cm^2 beryllium target. The FRS was tuned to the magnetic rigidity of projectile fragments with A/Z=2. Left: The isotopes reaching the final focus of the FRS are clearly identified via energy loss and time-of-flight (flight path 34.4 m). Right: Position of A/Z=2 beams in the direction of dispersion at the final focus of the FRS. The inclination is due to the fact that the tuning of the separator was not fully achromatic.

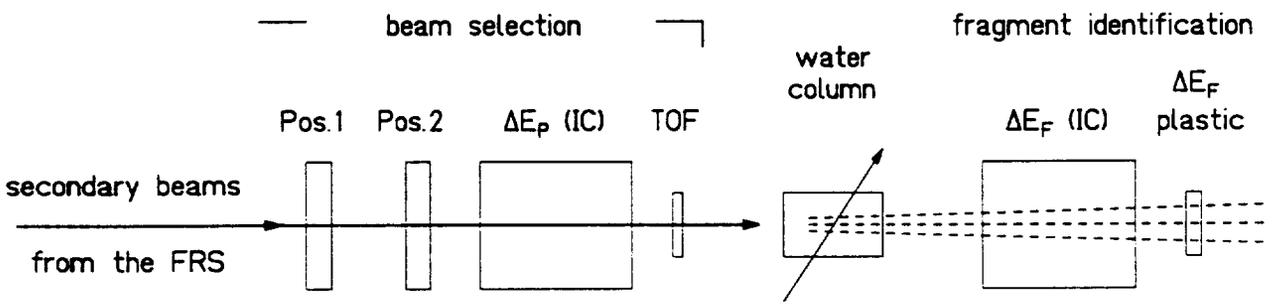

Fig. 2: Experimental set-up (in air) at the final focus of the FRS. The secondary beam particles were selected event-by-event via energy loss, time-of-flight and position-sensitive detectors before hitting a water target of variable thickness. The fragment Z-spectra were measured by a large-area ionisation chamber and a plastic scintillator.

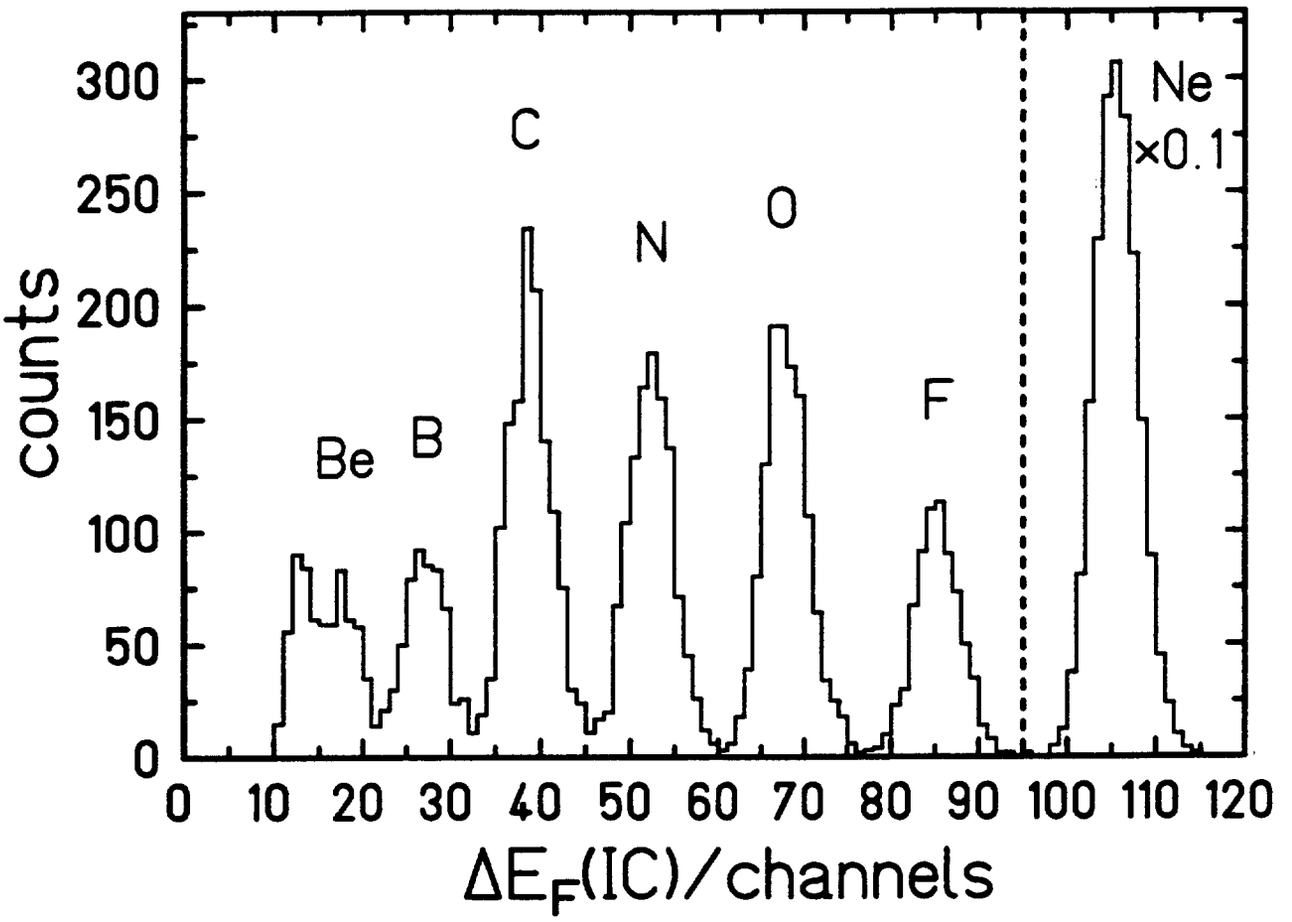

Fig. 3: Energy-loss spectrum of a 396 MeV/u ^{20}Ne beam behind a 4.2 cm thick water absorber measured with the ionisation chamber. The nuclear charge composition of the fragmented beam is clearly resolved down to Z=5.

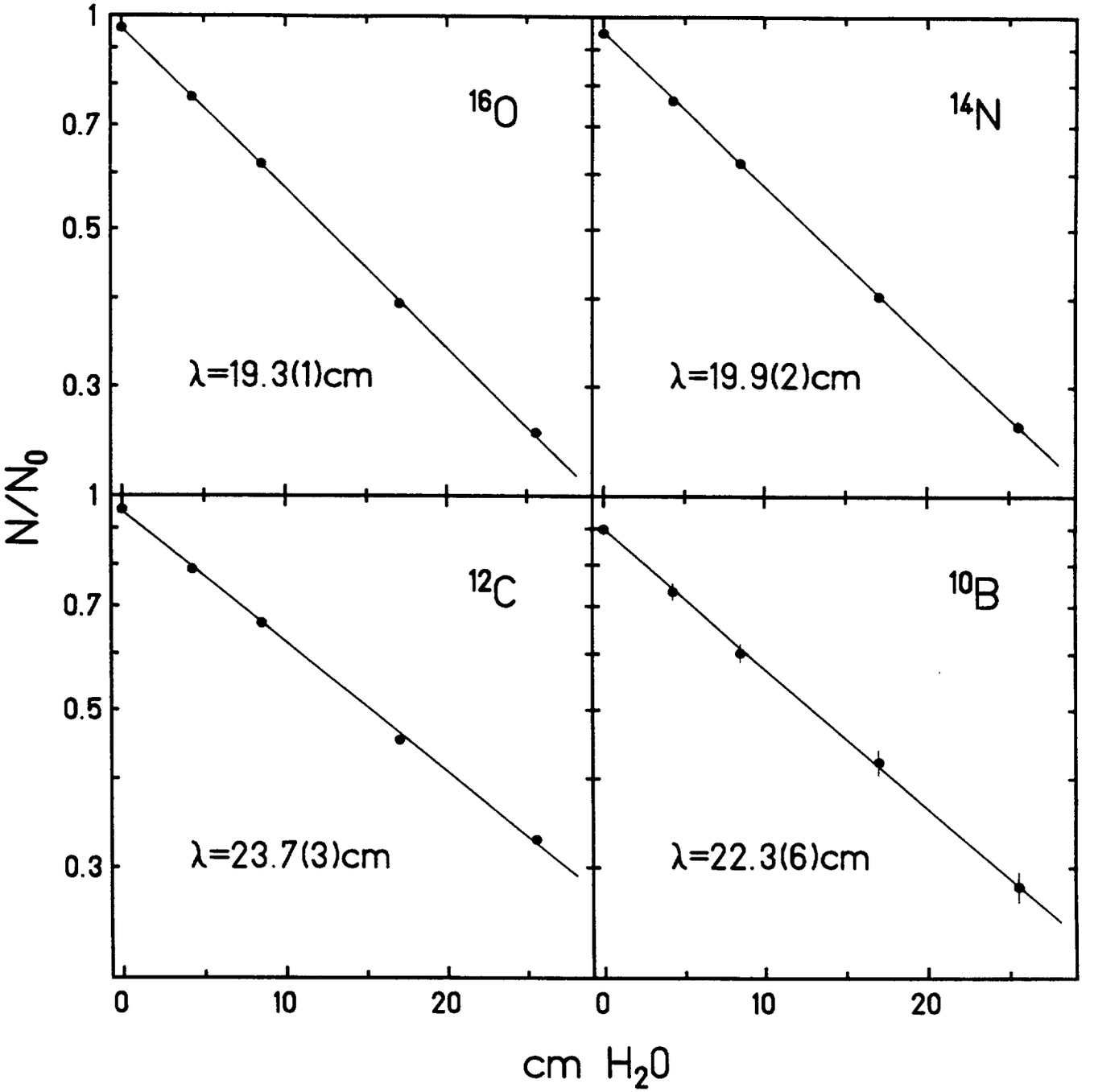

Fig. 4: Attenuation in water for beams of ^{16}O, ^{14}N, ^{12}C, and ^{10}B with an incident energy of about 670 MeV/u. The mean free path length λ results from fitting a one-component exponential to the data (see also Table 1).

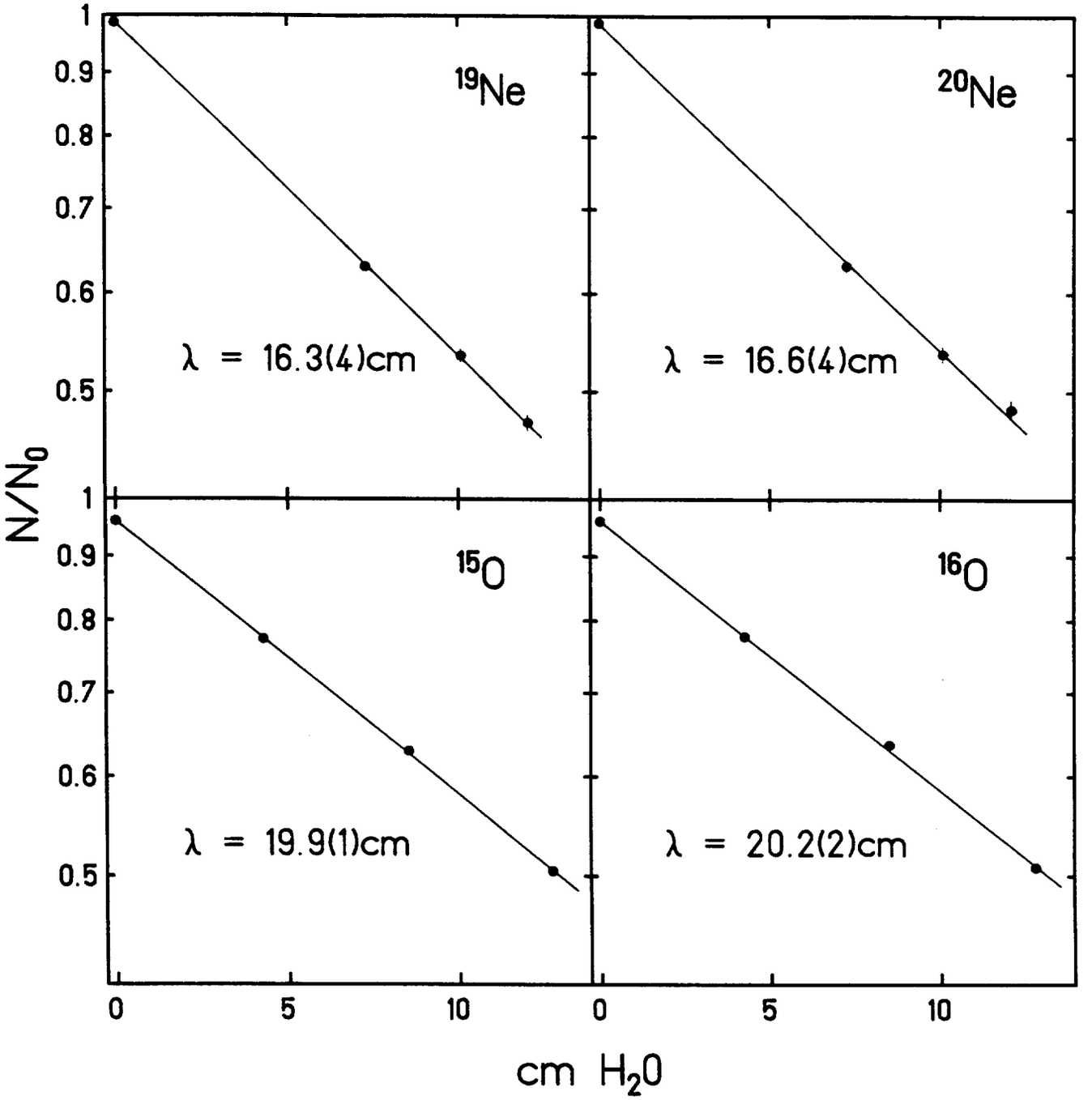

Fig. 5: Attenuation in water for stable and radioactive neon and oxygen beams with incident energies of 400 MeV/u (^{19}Ne), 405 MeV/u (^{20}Ne), 463 MeV/u (^{15}O), and 469 MeV/u (^{16}O).

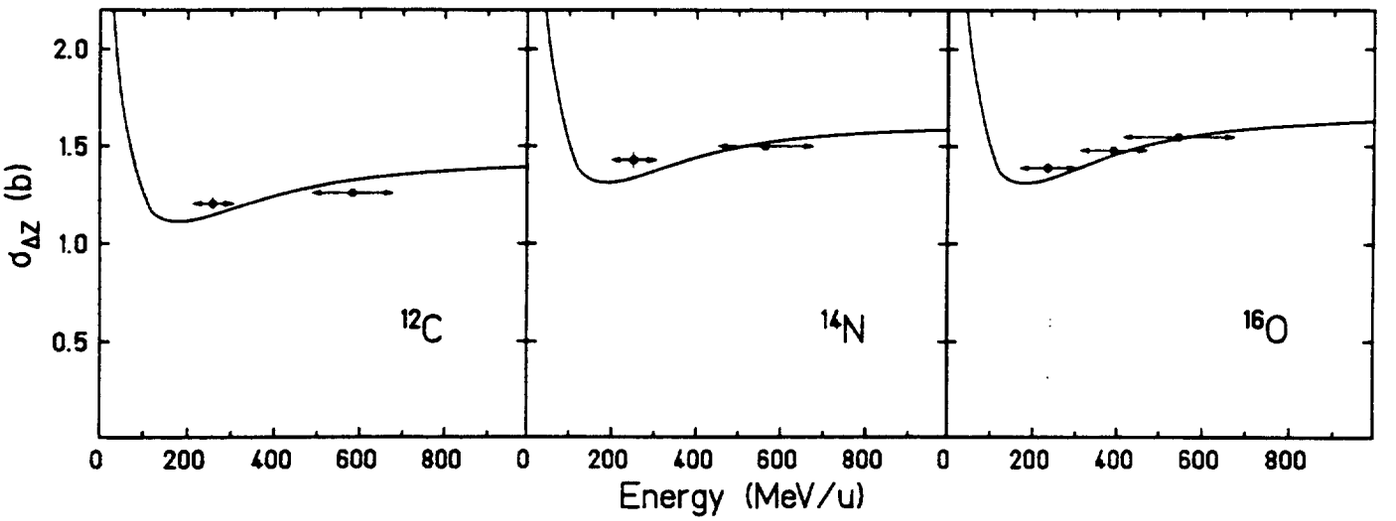

Fig. 6: Total charge-changing cross sections for ^{12}C, ^{14}N, ^{16}O beams in water. The experimental results for $\sigma^{tot.}_{\Delta Z}$ were obtained for several energy ranges indicated by arrows. The solid lines are predictions of the semiempirical model of Sihver et al. [41].

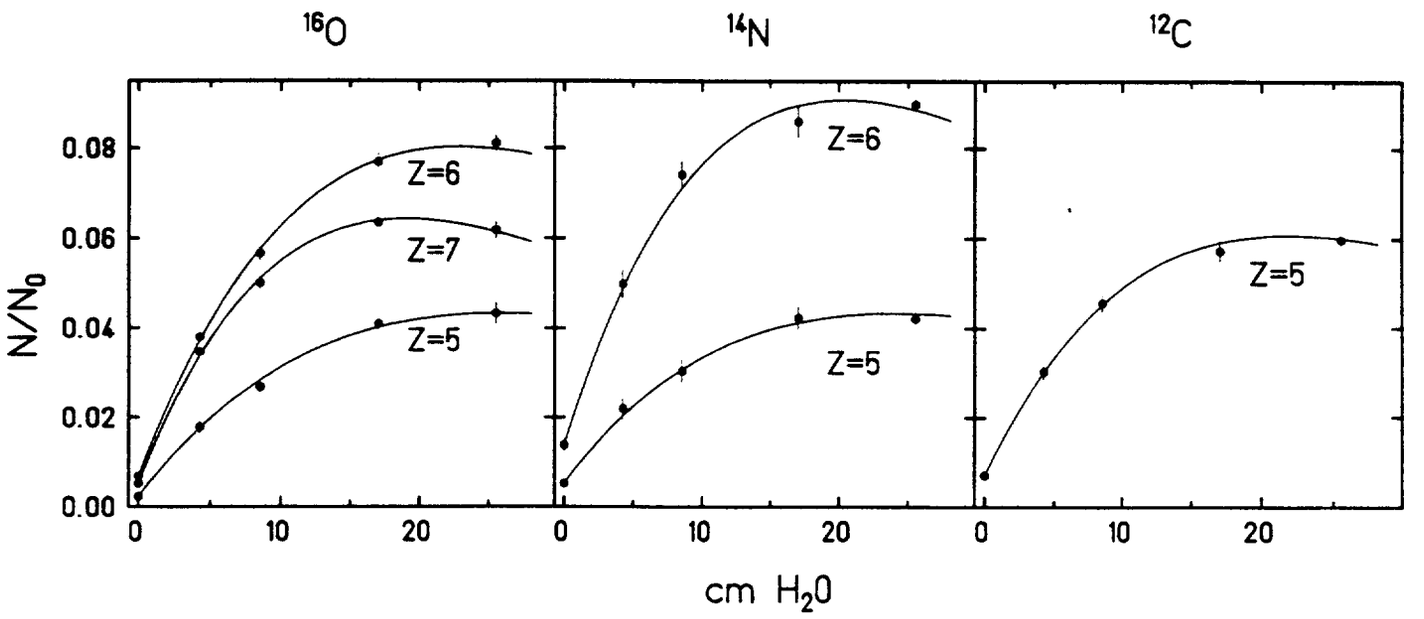

Fig. 7: Build-up of projectile fragments along the penetration path of ^{16}O, ^{14}N and ^{12}C beams in water ($E_{in} \sim 670$ MeV/u). The relative number of fragments with nuclear charge Z_f=7, 6, and 5 per incident beam particle is plotted as a function of water depth. The offset of fragmented beam particles at zero water depth is due to some additional matter in the beamline (TOF-detector, air gaps etc.).

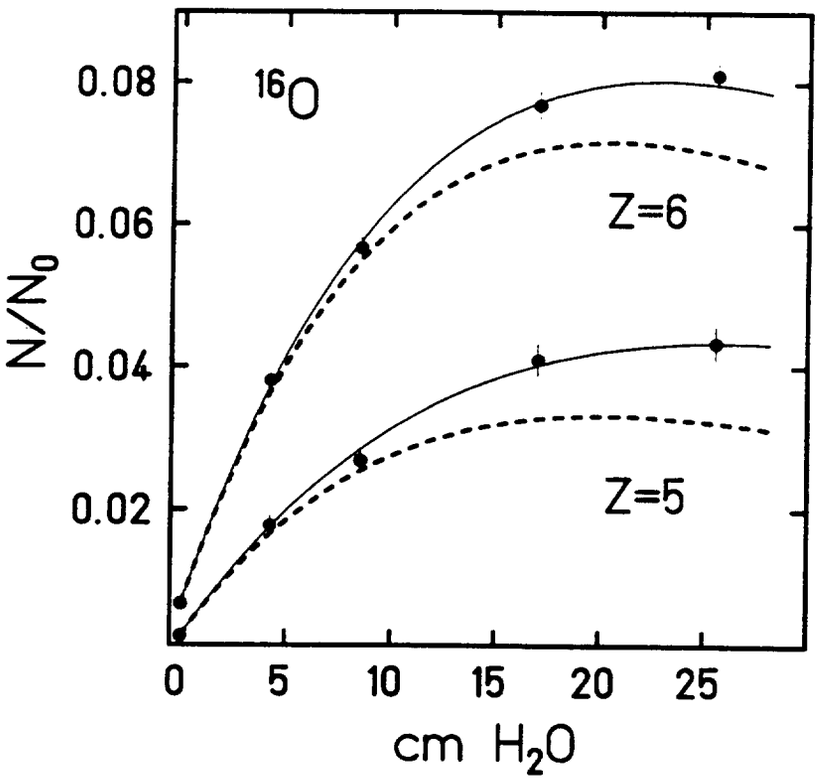

Fig. 8: The importance of higher-order generations in the fragmentation of an ^{16}O-beam in water. The build-up of Z=5 and Z=6 fragments is well reproduced by the fit taking into account all fragment generations (full line). The contribution of the first fragment generation alone is shown as a dashed line.